JACS
JOURNAL OF THE AMERICAN CHEMICAL SOCIETY
Article
pubs.acs.org/JACS

Electrochemical Detection of Transient Cobalt Hydride Intermediates of Electrocatalytic Hydrogen Production

Eric S. Wiedner* and R. Morris Bullock

Center for Molecular Electrocatalysis, Pacific Northwest National Laboratory, P.O. Box 999, K2-57, Richland, Washington 99352, United States

Supporting Information

ABSTRACT: A large variety of molecular cobalt complexes are used as electrocatalysts for H_2 production, but the key cobalt hydride intermediates are frequently difficult to detect and characterize due to their high reactivity. We report that a combination of variable scan rate cyclic voltammetry and foot-of-the-wave analysis (FOWA) can be used to detect transient $Co^{III}H$ and $Co^{II}H$ intermediates of electrocatalytic H_2 production by $[Co^{II}(P^{tBu}_2N^{Ph}_2)(CH_3CN)_3]^{2+}$ and $Co^{II}(dmgBF_2)_2(CH_3CN)_2$. In both cases, reduction of a transient catalytic intermediate occurs at a potential that coincides with the $Co^{II/I}$ couple. Each reduction displays quasireversible electron-transfer kinetics, consistent with reduction of a $Co^{III}H$ intermediate to $Co^{II}H$, which is then protonated by acid to generate H_2. A bridge-protonated Co^{I} species was ruled out as a catalytic intermediate for $Co^{II}(dmgBF_2)_2(CH_3CN)_2$ from voltammograms recorded at 1000 psi of H_2. Density functional theory was used to calculate Co^{III}–H and Co^{II}–H bond strengths for both catalysts. Despite having very different ligands, the cobalt hydrides of both catalysts possess nearly identical heterolytic and homolytic Co–H bond strengths for the $Co^{III}H$ and $Co^{II}H$ intermediates.

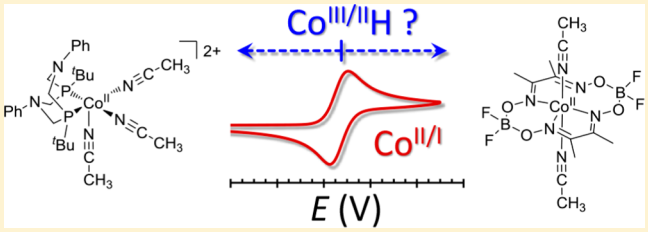

INTRODUCTION

Molecular cobalt complexes are widely studied as catalysts for electrocatalytic and photocatalytic production of H_2.[1−6] Many cobalt catalysts display desirable catalytic properties, including low overpotential,[7−11] solubility in water,[10,12−22] and stability toward O_2.[23−26] Several groups have constructed hybrid systems for production of H_2 in which a molecular cobalt catalyst has been attached to an electrode surface,[27−31] covalently linked to a photosensitizer,[32−36] or inserted into Photosystem I.[37]

In light of the popularity of cobalt catalysts for production of H_2, determination of the mechanism is crucial for the rational design of improved catalysts. Cobalt(III) monohydrides, $Co^{III}H$, can be formed by protonation of Co^{I} and are generally accepted as key intermediates in the catalytic formation of H_2.[1,4,19] Formation of H_2 from $Co^{III}H$ has been proposed to occur by either heterolytic or homolytic cleavage of the Co^{III}–H bond, or by reduction of $Co^{III}H$ to $Co^{II}H$, which can then form H_2 in a heterolytic or homolytic manner (Scheme 1).

Scheme 1. Potential Pathways for Formation of H_2

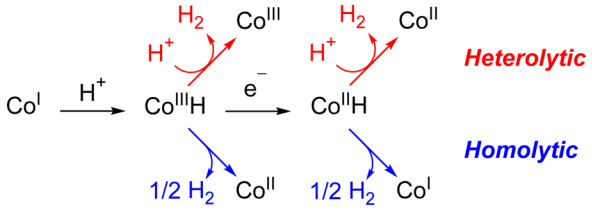

Determination of the $Co^{III}H$ reduction potential is critical for identification of the mechanism(s), as this will indicate the potential at which $Co^{II}H$ becomes a viable catalytic intermediate.

For some cobalt electrocatalysts, $Co^{III}H$ intermediates can be isolated or generated and characterized in situ.[38−42] In these cases, the reduction of $Co^{III}H$ to $Co^{II}H$ is readily identified by cyclic voltammetry and occurs at potentials more negative than the parent $Co^{II/I}$ couple. In the presence of an acid, the electrocatalytic wave appears at or slightly positive of the $Co^{III}H$ reduction wave, indicating that reduction to $Co^{II}H$ is required for catalysis.

In contrast to the behavior described above, many catalysts show an electrocatalytic wave near the $Co^{II/I}$ couple when moderate to strong acids are employed, suggesting either a difference in mechanism or that the potential of the $Co^{III/II}H$ couple coincides with the $Co^{II/I}$ couple. This situation is commonly encountered for $[Co^{II}(P^{tBu}_2N^{Ph}_2)(CH_3CN)_3]^{2+}$ (**1**)[43,44] and the well-known complex $Co^{II}(dmgBF_2)_2(CH_3CN)_2$ (**2**),[7−9,45,46] as well as related polyimine/polypyridyl catalysts.[12,13,17,22,47,48] The difficulty in studying the mechanism of these catalysts is epitomized by the debate regarding the H_2 production mechanism of **2**.[7,9,19] At present, the most commonly accepted mechanism for H_2 production by **2**, protonation of $Co^{II}H$, is supported by computations[49,50] and transient spectroscopic studies utilizing a very strong photoacid

Received: May 9, 2016
Published: June 14, 2016

DOI: 10.1021/jacs.6b04779
J. Am. Chem. Soc. 2016, 138, 8309−8318

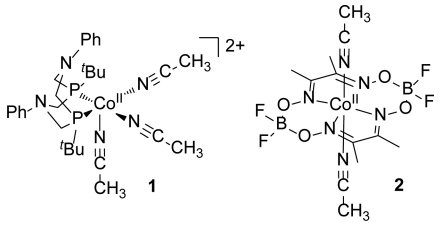

(pK_a = −26 in acetonitrile);[51] however, recent studies from Norton[52] and from Peters[53] have called into question the role of a $Co^{III}H$ intermediate during H_2 production.

A need clearly exists for widely applicable methods for identification and analysis of electrocatalytic mechanisms, both for $Co^{II}(dmgBF_2)_2(CH_3CN)_2$ as well as other catalysts. Costentin and Savéant have recently described a series of diagnostic electrochemical criteria for identification of various electrocatalytic mechanisms.[54,55] While useful as an initial assessment of the mechanism, these criteria do not provide structural information on catalytic intermediates, and can lead to ambiguous mechanistic conclusions in cases where the catalytic behavior is consistent with multiple mechanisms.

Herein we demonstrate that mechanistic information for $[Co^{II}(P^{tBu}{}_2N^{Ph}{}_2)(CH_3CN)_3]^{2+}$ and $Co^{II}(dmgBF_2)_2(CH_3CN)_2$ can be obtained under electrocatalytic conditions by using a combination of scan-rate variation and foot-of-the-wave analysis (FOWA).[56] Using these simple techniques, we have observed a transient intermediate that displays quasireversible electron-transfer kinetics for each catalyst, consistent with our prior studies on $Co^{III/II}H$ couples of isolated $Co^{III}H$ complexes.[39,57] Additionally, we report a thermodynamic analysis on Co−H bond strengths for both $[Co^{II}(P^{tBu}{}_2N^{Ph}{}_2)(CH_3CN)_3]^{2+}$ and $Co^{II}(dmgBF_2)_2(CH_3CN)_2$, providing insight into the similarities and differences of these two catalysts.

RESULTS

Electrochemical Analysis of $[Co^{II}(P^{tBu}{}_2N^{Ph}{}_2)(CH_3CN)_3]^{2+}$.

The identification of slow electron-transfer kinetics is first illustrated by examining the effect of scan rate on the $Co^{III/II}$ couple of $[Co^{II}(P^{tBu}{}_2N^{Ph}{}_2)(CH_3CN)_3]^{2+}$. Figure 1A shows cyclic voltammograms of $[Co^{II}(P^{tBu}{}_2N^{Ph}{}_2)(CH_3CN)_3]^{2+}$ in an acetonitrile solution in which the current has been normalized to $\nu^{-1/2}$ to facilitate comparison between voltammograms recorded at different scan rates. A reversible $Co^{II/I}$ couple is observed at $E_{1/2}$ = −0.87 V vs $Cp_2Fe^{+/0}$ (the reference couple for all potentials in this paper) with a peak-to-peak separation (ΔE_p) of 66 mV at ν = 0.1 V s^{-1}, close to the ideal ΔE_p = 57 mV expected for a Nernstian one-electron wave. The $Co^{III/II}$ couple is quasireversible with an $E_{1/2}$ = +0.33 V and a large ΔE_p = 128 mV. Increasing ν from 0.1 to 1.0 V s^{-1} (Figure 1A, dotted red trace) leads to a negligible increase in ΔE_p of the $Co^{II/I}$ couple, while a large increase of 120 mV is observed for the ΔE_p of the $Co^{III/II}$ couple. A plot of the anodic peak potential (E_{pa}) for the $Co^{III/II}$ wave versus log(ν) affords a slope of +57 mV, while the analogous plot of the cathodic peak potential (E_{pc}) versus log(ν) gives a slope of −57 mV (Figure 1B). These slopes are much larger than the value of ±20−30 mV expected for a peak variation due solely to a coupled chemical reaction, which further indicates that the $Co^{III/II}$ couple is influenced by electron-transfer kinetics.[58,59]

Two key electrochemical parameters for electron transfer are the standard heterogeneous electron-transfer rate constant, k_s (units of cm s^{-1}), and the transfer coefficient, α, which is a unitless term describing the symmetry of the energy barrier

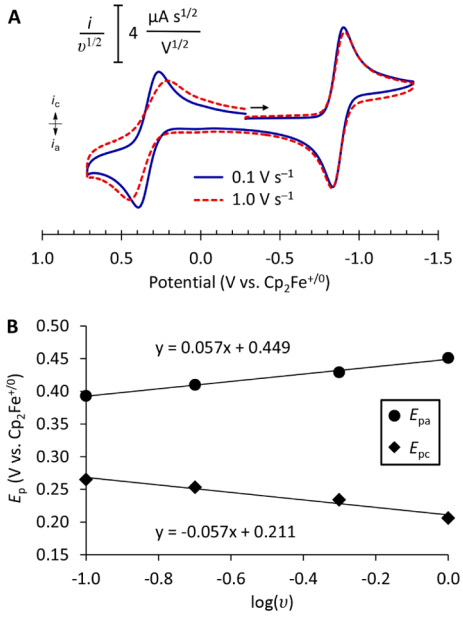

Figure 1. (A) Cyclic voltammograms of $[Co^{II}(P^{tBu}{}_2N^{Ph}{}_2)(CH_3CN)_3]^{2+}$ at varying scan rates. The current has been normalized to $\nu^{-1/2}$ to allow ready comparison of voltammograms recorded at different scan rates. (B) Plots of E_{pa} and E_{pc} of the $Co^{III/II}$ couple versus log(ν) over the range of 0.1−1.0 V s^{-1}. Conditions: 1 mM [Co] in 0.2 M NBu_4BF_4 acetonitrile, 1 mm diameter glassy carbon working electrode.

for electron transfer (α = 0.5 for a perfectly symmetrical barrier).[58,59] These two parameters are related to E_{pc} and E_{pa} by eqs 1 and 2,

$$E_{pc} = E^{\circ\prime} - \frac{0.78RT}{\alpha F} + \frac{2.303RT}{\alpha F}\log\left(k_s\sqrt{\frac{RT}{\alpha F\nu D}}\right) \quad (1)$$

$$E_{pa} = E^{\circ\prime} + \frac{0.78RT}{\alpha F} - \frac{2.303RT}{(1-\alpha)F}\log\left(k_s\sqrt{\frac{RT}{(1-\alpha)F\nu D}}\right) \quad (2)$$

where $E^{\circ\prime}$ is the formal reduction potential of the electron transfer, R is the gas constant, T is the temperature in K, F is the Faraday constant, and D is the diffusion coefficient of the analyte in cm^2 s^{-1}. The observation of equivalent slopes in the E_p versus log(ν) plots indicates that α = 0.5 for the $Co^{III/II}$ couple of $[Co^{II}(P^{tBu}{}_2N^{Ph}{}_2)(CH_3CN)_3]^{2+}$, and a value of k_s = 0.003 cm s^{-1} is obtained from eqs 1 and 2 using E° = +0.33 V and D = 8.2 × 10^{-6} cm^2 s^{-1} (see the Supporting Information (SI) for more details). This value of k_s is approximately 2 orders of magnitude smaller than the value of k_s = 0.25 cm s^{-1} reported for the ferrocenium/ferrocene couple in acetonitrile using a glassy carbon electrode,[60] which emphasizes the slow electron-transfer kinetics of the $Co^{III/II}$ couple.

Electrochemical reduction of Co^{II} to Co^{I} in the presence of acid is expected to form CoH intermediates. Cyclic voltammograms were recorded on $[Co^{II}(P^{tBu}{}_2N^{Ph}{}_2)(CH_3CN)_3]^{2+}$ in the presence of 4 equiv of *p*-bromoanilinium (pK_a = 9.43)[61] in acetonitrile (Figure 2A). At a slow scan rate of 0.1 V s^{-1}, the catalytic wave displays a peak (E_{pc} = −0.98 V) that is 110 mV negative of the $Co^{II/I}$ couple, and an anodic wave corresponding to oxidation of Co^{I} is observed on the return scan. Increasing ν causes the E_{pc} of the catalytic wave to shift negative until it separates from the $Co^{II/I}$ couple at ν = 2 V s^{-1}.

DOI: 10.1021/jacs.6b04779
J. Am. Chem. Soc. 2016, 138, 8309−8318

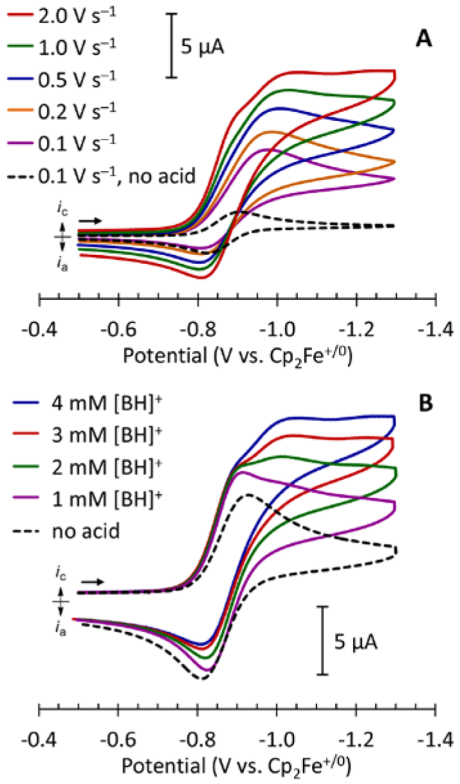

Figure 2. (A) Cyclic voltammograms of $[Co^{II}(P^{tBu}{}_2N^{Ph}{}_2)(CH_3CN)_3]^{2+}$ (1 mM) and *p*-bromoanilinium tetrafluoroborate (4 mM) at varying scan rates. (B) Cyclic voltammograms of $[Co^{II}(P^{tBu}{}_2N^{Ph}{}_2)(CH_3CN)_3]^{2+}$ (1 mM) and varying concentrations of *p*-bromoanilinium tetrafluoroborate (1–4 mM) at ν = 2 V s^{-1}. Conditions: 0.2 M NBu_4BF_4 acetonitrile, 1 mm diameter glassy carbon working electrode.

The separation of the $Co^{II/I}$ couple and the catalytic wave is more clearly observed in voltammograms recorded at ν = 2 V s^{-1} with increasing amounts of *p*-bromoanilinium (Figure 2B), in which the current at the $Co^{II/I}$ couple remains constant while the intensity of the catalytic wave (E_{pc} = −1.04 V) continues to increase with the acid concentration. These data indicate that a species other than $[Co^{II}(P^{tBu}{}_2N^{Ph}{}_2)(CH_3CN)_3]^{2+}$ must be reduced prior to formation of H_2, and we attribute this process to reduction from $Co^{III}H$ to $Co^{II}H$.

The electron-transfer kinetics of the proposed $Co^{III}H$ intermediate were investigated from plots of E_{pc} for the catalytic wave versus log(ν). A slope of −54 mV was obtained from the plot of E_{pc} versus log(ν) using 4 equiv of *p*-bromoanilinium (SI, Figure S1), which affords $\alpha \approx 0.5$ for the presumed $Co^{III/II}H$ couple according to eq 1. A value for k_s of the $Co^{III/II}H$ couple could not be obtained from these data since the absence of a return wave for oxidation of $Co^{II}H$ precludes an accurate determination of $E^{\circ\prime}$. However, the presence of electron-transfer kinetic limitations is apparent from the value of the slope in the E_{pc} versus log(ν) plot, consistent with reduction of a $Co^{III}H$ intermediate.

Foot-of-the-wave analysis (FOWA)[56] was used to gain further insight into the proximity of the $Co^{III/II}H$ and $Co^{II/I}$ couples of $[Co^{II}(P^{tBu}{}_2N^{Ph}{}_2)(CH_3CN)_3]^{2+}$. In FOWA, the electrocatalytic wave is analyzed according to eq 3, where i_p is the peak current of the reversible non-catalytic wave, i_{cat} is the steady-state catalytic plateau current, $E_{cat/2}$ is the potential at $i_{cat/2}$, and the expression $1/\{1 + \exp[(F/RT)(E - E_{cat/2})]\}$ describes the fraction of catalyst that is reduced at a given potential. In the absence of any competing side phenomena, a plot of i/i_p versus $1/\{1 + \exp[(F/RT)(E - E_{cat/2})]\}$ affords a straight line with an intercept of zero and a slope equal to i_{cat}/i_p. A requirement for this linear relationship is that one of the electron transfers for catalysis should occur at a much more positive potential than the other, i.e., a large $\Delta E^{\circ\prime}$.[54,62] This requirement is not fulfilled for $[Co^{II}(P^{tBu}{}_2N^{Ph}{}_2)(CH_3CN)_3]^{2+}$, as the $Co^{II/I}$ and $Co^{III/II}H$ couples occur at similar potentials; as a result, this catalyst should not display ideal FOWA behavior. Note that eq 3 is distinct from an alternate implementation of FOWA in which $E_{1/2}$ of the non-catalytic wave is used instead of $E_{cat/2}$. When using $E_{1/2}$ in FOWA, a linear FOWA plot is only observed when the first chemical step is rate-limiting.[54,62]

$$\frac{i}{i_p} = \frac{i_{cat}/i_p}{1 + \exp\left[\frac{F}{RT}(E - E_{cat/2})\right]} \quad (3)$$

A FOWA plot for $[Co^{II}(P^{tBu}{}_2N^{Ph}{}_2)(CH_3CN)_3]^{2+}$ shows three distinct regions (Figure 3A). The normalized current increases rapidly at small values of $1/\{1 + \exp[(F/RT)(E - E_{cat/2})]\}$, then obtains a constant slope at intermediate values of $1/\{1 + \exp[(F/RT)(E - E_{cat/2})]\}$, corresponding to the idealized FOWA behavior. Finally, the current drops off rapidly at high $1/\{1 + \exp[(F/RT)(E - E_{cat/2})]\}$ due to acid depletion near the peak of the catalytic wave. The linear FOWA region can be mapped onto the CV of $[Co^{II}(P^{tBu}{}_2N^{Ph}{}_2)(CH_3CN)_3]^{2+}$ (Figure 3B), showing that both the foot and the peak of the wave are affected by competing phenomena.

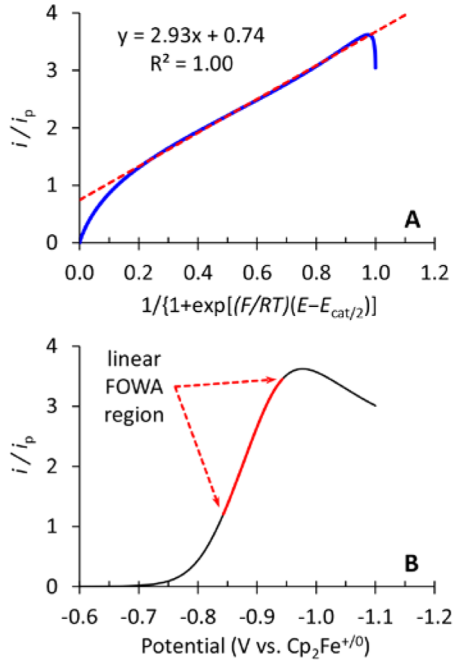

Figure 3. (A) FOWA plot (solid blue trace) of $[Co^{II}(P^{tBu}{}_2N^{Ph}{}_2)(CH_3CN)_3]^{2+}$ showing the linear fit (dashed red line). (B) Normalized cyclic voltammogram (black trace) showing the potential window that affords a linear FOWA plot (red trace). Conditions: 1 mM $[Co^{II}(P^{tBu}{}_2N^{Ph}{}_2)(CH_3CN)_3]^{2+}$, 4 mM *p*-bromoanilinium tetrafluoroborate, 0.2 M NBu_4BF_4 acetonitrile, ν = 0.1 V s^{-1}.

The non-ideal FOWA behavior observed at the foot of the wave indicates that the $Co^{III/II}H$ couple is more negative than the $Co^{II/I}$ couple. The initial current increase corresponds to stoichiometric reduction of Co^{II}, and i/i_p does not exceed unity

DOI: 10.1021/jacs.6b04779
J. Am. Chem. Soc. 2016, 138, 8309–8318

until the potential becomes negative enough for $Co^{III}H$ reduction, and hence catalysis, to be kinetically feasible. Therefore, FOWA of $[Co^{II}(P^{tBu}{}_2N^{Ph}{}_2)(CH_3CN)_3]^{2+}$ provides similar mechanistic information as the scan rate analysis, but FOWA is not contingent upon the $Co^{III/II}H$ couple having slow electron-transfer kinetics.

Electrochemical Analysis of $Co^{II}(dmgBF_2)_2(CH_3CN)_2$. Scan rate analysis of $Co^{II}(dmgBF_2)_2(CH_3CN)_2$ in acetonitrile shows a quasireversible $Co^{III/II}$ couple, and plots of E_{pa} and E_{pc} versus $\log(\nu)$ for the $Co^{III/II}$ couple afford slopes of 82 and −58 mV (SI, Figures S2 and S3). While these plots do not conform precisely to eqs 1 and 2, analysis provides approximate values of $E^{\circ\prime}$ = +0.14 V, α = 0.6, and $k_s = 2 \times 10^{-5}$ cm s^{-1} (see the SI for more details). These values are similar to those measured from steady-state voltammograms of $Co^{II}(dmgBF_2)_2(CH_3CN)_2$ using a Pt rotating disc electrode.[63]

As with $[Co^{II}(P^{tBu}{}_2N^{Ph}{}_2)(CH_3CN)_3]^{2+}$, CoH intermediates arising from $Co^{II}(dmgBF_2)_2(CH_3CN)_2$ were generated by recording cyclic voltammograms in the presence of 4 equiv of anilinium tetrafluoroborate (pK_a = 10.62 in CH_3CN)[61] over a range of ν (Figure 4). Under these conditions, a peak-shaped

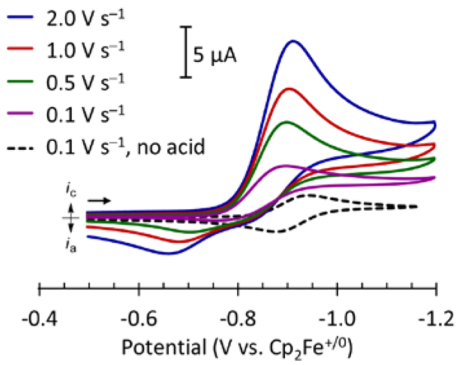

Figure 4. Cyclic voltammograms of $Co^{II}(dmgBF_2)_2(CH_3CN)_2$ (1 mM) and anilinium tetrafluoroborate (4 mM) at varying scan rates. Conditions: 0.2 M NBu_4BF_4 acetonitrile, 1 mm diameter glassy carbon working electrode.

catalytic wave (E_{pc} = −0.90 V) is observed at a potential slightly positive of the $Co^{II/I}$ couple ($E_{1/2}$ = −0.91 V). An anodic wave for oxidation of Co^{I} is not observed under these conditions, indicating that its steady-state concentration within the diffusion layer is low. A new anodic wave (E_{pa} = −0.71 V) appears on the return sweep at ν = 0.5 V s^{-1}, and this wave shifts to more positive potentials as ν is increased further. A plot of E_{pa} versus $\log(\nu)$ afforded a slope of 73 mV (SI, Figure S4), indicating that the potential of this oxidation wave is governed by electron-transfer kinetics. The oxidation wave can be tentatively assigned to oxidation of a CoH intermediate on the return sweep; however, the lack of distinct features on the forward cathodic sweep does not reveal whether the initial $Co^{III}H$ species is reduced to $Co^{II}H$, so the anodic wave on the return sweep could correspond to oxidation of either $Co^{II}H$ or $Co^{III}H$.

FOWA of $Co^{II}(dmgBF_2)_2(CH_3CN)_2$ was employed to further investigate whether the initially formed $Co^{III}H$ intermediate is reduced at potentials near the $Co^{II/I}$ couple. A linear FOWA plot was observed over most of the range of $1/\{1 + \exp[(F/RT)(E - E_{cat/2})]\}$, with acid depletion causing a sharp decline in i/i_p at high $1/\{1 + \exp[(F/RT)(E - E_{cat/2})]\}$ (Figure 5A). Close examination of the FOWA plot reveals that i/i_p increases more slowly at the onset of the catalytic wave

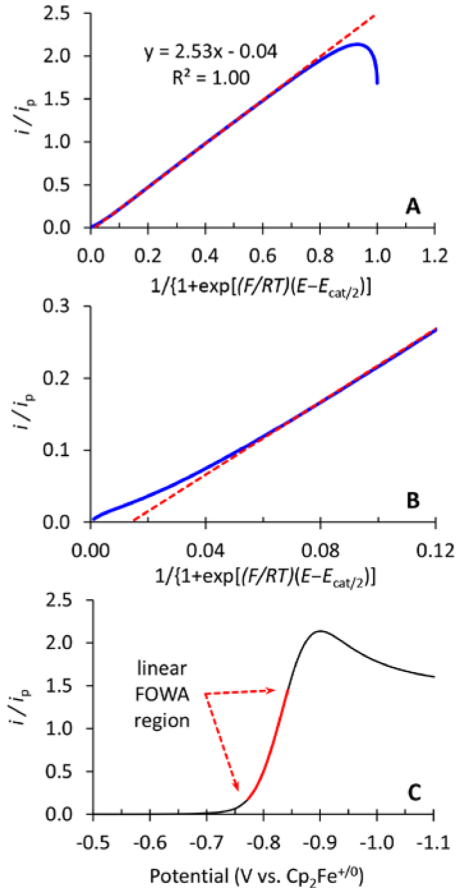

Figure 5. (A) FOWA plot (solid blue trace) of $Co^{II}(dmgBF_2)_2(CH_3CN)_2$ showing the linear fit (dashed red line). (B) Expansion of the FOWA plot showing the deviation from linearity at low i/i_p. (C) Normalized cyclic voltammogram (black trace) showing the potential window that affords a linear FOWA plot (red trace). Conditions: 1 mM $Co^{II}(dmgBF_2)_2(CH_3CN)_2$, 4 mM *p*-bromoanilinium tetrafluoroborate, 0.2 M NBu_4BF_4 acetonitrile, ν = 0.1 V s^{-1}.

(Figure 5B,C), indicating that catalysis is slower at the foot of the wave. This observation reveals that the initial $Co^{III}H$ intermediate must be reduced for catalysis to occur, and that its reduction potential is near the potential at the foot of the wave. Thus, $Co^{II}H$ is the catalytically active species leading to H_2 formation, and is oxidized back to $Co^{III}H$ on the return anodic sweep.

While the FOWA reveals that $Co^{III}H$ must be reduced for catalysis to proceed, it does not indicate the mechanism by which the reduction occurs. For example, $Co^{III}H$ could be reduced directly by the electrode or by an equivalent of Co^{I} in a solution electron-transfer pathway.[54] Regardless of the electron-transfer mechanism, the $Co^{III}H$ intermediate must be reduced to a $Co^{II}H$ species prior to formation of H_2.

A value of $E^{\circ\prime} \approx -0.75$ V was determined for the $Co^{III/II}H$ couple using the peak potentials estimated from FOWA and slow scan rate CVs. This estimated value for the $Co^{III/II}H$ couple is 160 mV more positive than the $Co^{II/I}$ couple, and is 140 mV more positive than the computationally predicted $Co^{III/II}H$ reduction potential of −0.89 V.[50] Estimates of α = 0.6 and $k_s = 7 \times 10^{-3}$ cm s^{-1} can be made for the $Co^{III/II}H$ couple using $E^{\circ\prime}$ and the dependence of E_{pa} on $\log(\nu)$ discussed above.

Thus, far we have postulated that the transient intermediate is best described as $Co^{III}H$ based on the observation of

DOI: 10.1021/jacs.6b04779
J. Am. Chem. Soc. 2016, 138, 8309−8318

quasireversible electron-transfer kinetics. An alternative possibility is that Co^{I} is protonated on an oxygen atom of the $dmgBF_2$ ligand instead of at Co, forming a bridge-protonated Co^{I} intermediate. This intermediate would be analogous to the complex recently observed by Norton and co-workers from the reaction of $Co^{II}(dmgBF_2)_2(CH_3CN)_2$ with high pressures of H_2; this reaction was proposed to proceed by tautomerization of an initial $Co^{III}H$ intermediate (eq 4).[52]

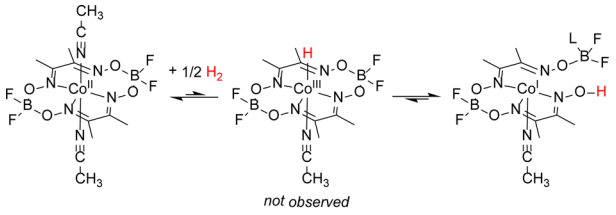

(4)

Voltammograms of $Co^{II}(dmgBF_2)_2(CH_3CN)_2$ were recorded at high pressures of H_2 to characterize the Norton product electrochemically and compare it to the intermediates formed under electrocatalytic conditions. At 1000 psi of H_2, the current of the $Co^{II/I}$ couple gradually diminishes over 48 h, and is accompanied by the appearance of a new quasireversible reduction wave centered at $E_{1/2} = -1.21$ V (Figure 6). The new

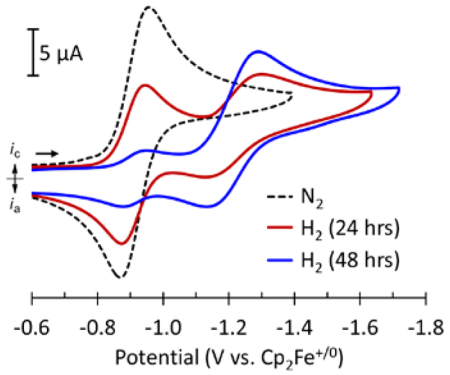

Figure 6. Cyclic voltammograms of $Co^{II}(dmgBF_2)_2(CH_3CN)_2$ (1 mM) under N_2 (dashed black trace), and 1000 psi H_2 after 24 h (red trace) and 48 h (blue trace). Conditions: 0.2 M NBu_4PF_6 acetonitrile solution, ν = 0.1 V s^{-1}, 1 mm diameter glassy carbon working electrode.

reduction feature slowly reverts back to the original $Co^{II/I}$ couple upon releasing the H_2 pressure (SI, Figure S16), demonstrating that the reaction product corresponds to the bridge-protonated Co^{I} species characterized by Norton. Notably, the reduction potential of the bridge-protonated product is 300 mV more negative than the $Co^{II/I}$ couple, indicating this species is not an intermediate of electrocatalytic proton reduction by $Co^{II}(dmgBF_2)_2(CH_3CN)_2$.

Thermochemical Analysis. To gain further insight into catalytic performance, the Co−H bond strengths of cobalt hydrides formed from $[Co^{II}(P^{tBu}{}_2N^{Ph}{}_2)(CH_3CN)_3]^{2+}$ were analyzed in terms of their acidity (pK_a), homolytic bond dissociation free energy (BDFE, $\Delta G^{\circ}_{H^{\bullet}}$), and hydride donor ability ($\Delta G^{\circ}_{H^{-}}$). A DFT isodesmic method was employed due to the transient nature of the CoH species. In the isodesmic method, the thermodynamic property of interest is calculated versus a reference system for which the same property is already known.[64] This method provides cancellation of the systematic errors of DFT values if the reference molecule is of similar structure to the compound of interest.[65−67] Multiple features of the reference system must be matched to obtain high accuracy, including the number and type of donor ligands, overall molecular charge, and the formal oxidation state of the metal.[40] With these considerations in mind, $[Co^{II}(dppe)_2(CH_3CN)]^{2+}$ (dppe = 1,2-bis(diphenylphosphino)ethane) was selected as a reference for $[Co^{II}(P^{tBu}{}_2N^{Ph}{}_2)(CH_3CN)_3]^{2+}$. Thermodynamic properties of $[Co^{II}(dppe)_2(CH_3CN)]^{2+}$ are well-established,[40,68] and this system has previously been shown to be a suitable reference for DFT isodesmic schemes.[40,50]

The reaction free energy was computed for hydride transfer from $[HCo^{II}(P^{tBu}{}_2N^{Ph}{}_2)(CH_3CN)_2]^{+}$ to $[Co^{II}(dppe)_2(CH_3CN)]^{2+}$ (eq 5). Each of the Co^{II} species in this reaction were calculated

$$[HCo^{II}(P^{tBu}{}_2N^{Ph}{}_2)(CH_3CN)_2]^{+} + [Co^{II}(dppe)_2(CH_3CN)]^{2+} \rightleftharpoons [Co^{II}(P^{tBu}{}_2N^{Ph}{}_2)(CH_3CN)_3]^{2+} + [HCo^{II}(dppe)_2]^{+} \quad (5)$$

to have 5-coordinate structures, so loss of a hydride ligand is accompanied by acetontirile binding. A thermodynamic hydricity of 54.2 kcal mol^{-1} was calculated for $[HCo^{II}(P^{tBu}{}_2N^{Ph}{}_2)(CH_3CN)_2]^{+}$ using the reaction free energy of eq 5 (−6.3 kcal mol^{-1}) and the known hydricity of $[HCo^{II}(dppe)_2]^{+}$ (60.5 kcal mol^{-1}).[40,68] In a similar manner, a reduction potential of −0.80 V was calculated for the $[HCo^{III}(P^{tBu}{}_2N^{Ph}{}_2)(CH_3CN)_3]^{2+}/[HCo^{II}(P^{tBu}{}_2N^{Ph}{}_2)(CH_3CN)_2]^{+}$ couple using the $[HCo^{III}(dppe)_2(CH_3CN)]^{2+}/[HCo^{II}(dppe)_2]^{+}$ couple as a reference. Combination of these two properties with the experimentally measured $E_{1/2}$ values for the $Co^{III/II}$ and $Co^{II/I}$ couples of $[Co^{II}(P^{tBu}{}_2N^{Ph}{}_2)(CH_3CN)_3]^{2+}$ allows calculation of additional heterolytic and homolytic Co−H bond strengths (Scheme 2) using known thermochemical cycles.[69,70]

A similar thermochemical scheme was constructed for $Co^{II}(dmgBF_2)_2(CH_3CN)_2$ using the newly determined $Co^{III/II}H$ reduction potential. A single Co−H bond strength is needed to determine the remaining Co−H bond strengths from thermochemical cycles using the experimental reduction potentials. A previous DFT study used a pK_a value of 13.3 for $HCo^{III}(dmgBF_2)_2(CH_3CN)$,[50] which was estimated by Artero and co-workers from digital simulations of catalytic voltammograms using a mechanism involving protonation of $Co^{III}H$ instead of $Co^{II}H$.[9] Rather than using this estimated pK_a value, we calculated the BDFE of $HCo^{III}(dmgBF_2)_2(CH_3CN)$ relative to $[HCo^{III}(dppe)_2(CH_3CN)]^{2+}$ using the isodesmic reaction shown in eq 6. While there is a difference in charge between the

$$HCo^{III}(dmgBF_2)_2(CH_3CN) + [Co^{II}(dppe)_2(CH_3CN)]^{2+} \rightleftharpoons Co^{II}(dmgBF_2)_2(CH_3CN) + [HCo^{III}(dppe)_2(CH_3CN)]^{2+} \quad (6)$$

$(dmgBF_2)_2{}^{2-}$ and $(dppe)_2$ ligand sets, the computational error should be minimal for this isodesmic reaction since it corresponds to transfer of a neutral $H^{\bullet}$ between two Co^{II} centers without a change in acetonitrile coordination. Additional heterolytic and homolytic Co−H bond strengths were determined from thermochemical cycles using the computed BDFE and the experimentally measured reduction potentials for the $Co^{III/II}$, $Co^{II/I}$, and $Co^{III/II}H$ couples (Scheme 2). These calculations afford a pK_a value of 10.7 for $HCo^{III}(dmgBF_2)_2(CH_3CN)$, which is 2.6 pK_a units (3.5 kcal mol^{-1}) lower than the previous estimate.

DOI: 10.1021/jacs.6b04779
J. Am. Chem. Soc. 2016, 138, 8309−8318

Scheme 2. Thermochemical Data for $[Co^{II}(P^{tBu}{}_2N^{Ph}{}_2)(CH_3CN)_3]^{2+}$, $Co^{II}(dmgBF_2)_2(CH_3CN)_2$, and Related Species in Acetonitrile Solution, Showing Relationships among $E^{\circ\prime}$, pK_a, $\Delta G^\circ_{H^-}$, and BDFE Values[a]

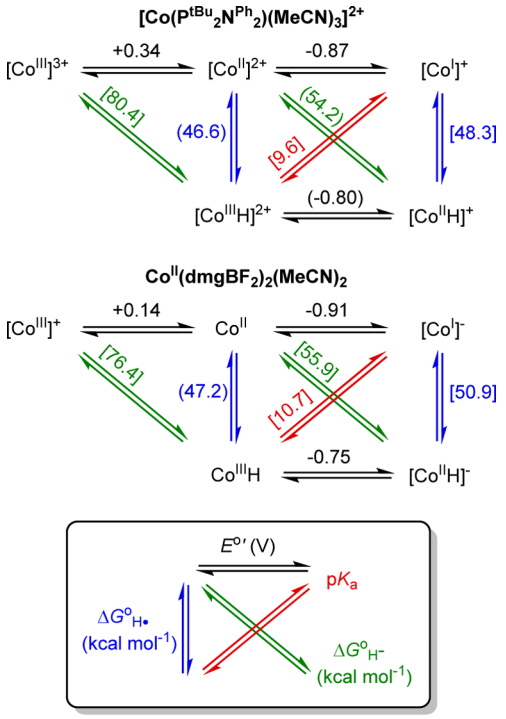

[a]Unbracketed values were determined experimentally, values in parentheses were calculated by a DFT isodesmic reaction, and values in square brackets were determined by completion of a thermochemical cycle.

The pK_a of 10.7 calculated for $HCo^{III}(dmgBF_2)_2(CH_3CN)$ is considerably lower than the pK_a of 13.4 measured for the bridge-protonated Co^I tautomer by Norton and co-workers.[52] This difference in pK_a values suggests an equilibrium constant of 500 for conversion of $Co^{III}H$ into the thermodynamically favored bridge-protonated Co^I complex (eq 4). The Co^I tautomer is not observed under electrocatalytic conditions, however, indicating that intramolecular migration of the proton from cobalt to the ligand is slow on the time scale required to record a CV (<20 s).

DISCUSSION

Determination of the Mechanism. Modeling of voltammograms using digital simulations has long been used to examine electrochemical mechanisms, but simulation does not always provide a unique solution. A leading example of this challenge can be found in early studies of $Co^{II}(dmgBF_2)_2(CH_3CN)_2$. Using digital simulation, Artero and co-workers concluded the catalytic mechanism to be protonation of $Co^{III}H$ to make H_2,[9] while Peters and co-workers concluded that a bimetallic reaction of two $Co^{III}H$ intermediates was more likely.[7] Furthermore, neither group proposed the currently accepted mechanism involving a $Co^{II}H$ intermediate, which highlights the limitations of digital simulation for mechanistic analysis.

Costentin and Savéant have presented electrochemical diagnostic criteria for distinguishing between different multielectron electrocatalytic mechanisms.[54,55] Their method is conceptually similar to digital simulation, except that the dependence of i_{cat} and $E_{cat/2}$ on the acid and catalyst concentration is analyzed instead of reproducing the entire catalytic wave. Using this methodology, Dempsey and co-workers very recently reported a kinetic study of electrocatalytic proton reduction by $Co^{II}(dmgBF_2)_2(CH_3CN)_2$ using anilinium acids as the proton source.[71] In this study the authors were able to rule out a bimetallic pathway for H_2 formation; however, they were unable to distinguish between an ECEC or ECCE mechanism using electrochemical analysis alone, as the diagnostic features of these two pathways are similar. As a result, the authors concluded an ECEC mechanism by relying on prior computational analysis[49,50] and time-resolved spectroscopic studies utilizing a very strong photoacid (pK_a = −26 in acetonitrile).[51]

Application of Costentin and Savéant's diagnostic criteria is even more ambiguous for $[Co^{II}(P^{tBu}{}_2N^{Ph}{}_2)(CH_3CN)_3]^{2+}$ than for $Co^{II}(dmgBF_2)_2(CH_3CN)_2$. In our previous study of $[Co^{II}(P^{tBu}{}_2N^{Ph}{}_2)(CH_3CN)_3]^{2+}$, the catalytic rate constant was found to be first-order in catalyst, first-order in acid at low acid concentrations, and independent of the acid concentration at elevated acid concentrations (>300 mM).[44] Since the electrocatalytic wave appears at the $Co^{II/I}$ couple, the kinetic data indicates the rate-limiting step is protonation of Co^I to make $Co^{III}H$, and kinetic information on the subsequent chemical steps cannot be measured from the electrochemical diagnostic criteria. As a result, the experimental data are consistent with four different mechanisms (Scheme 1): protonation of either $Co^{III}H$ or $Co^{II}H$ to form H_2, or bimolecular reaction of two $Co^{III}H$ or $Co^{II}H$ intermediates.[54,55]

The present method is complementary to the diagnostic criteria presented by Costentin and Savéant. Our strategy is to directly observe reduction steps that overlap with the catalytic wave under conditions of slow catalysis, i.e., very low concentrations of the acid. The low acid concentration increases the lifetime of the catalytic intermediates, which are then detected using electrochemical techniques. In this manner we have shown that both $[Co^{II}(P^{tBu}{}_2N^{Ph}{}_2)(CH_3CN)_3]^{2+}$ and $Co^{II}(dmgBF_2)_2(CH_3CN)_2$ proceed by sequential electron and proton transfers in an ECEC mechanism for H_2 production, consistent with protonation of a $Co^{II}H$ intermediate in a pathway involving heterolytic cleavage of the Co−H bond (Scheme 3).

Scheme 3. ECEC Mechanism for H_2 Formation by Protonation of $Co^{II}H$

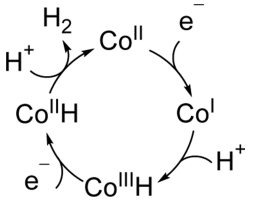

The resting state for each catalyst is readily determined from the potential of the anodic wave on the return sweep. Oxidation of Co^I is observed on the return sweep of $[Co^{II}(P^{tBu}{}_2N^{Ph}{}_2)(CH_3CN)_3]^{2+}$, indicating that protonation of Co^I is rate-limiting for catalysis. In contrast, a new anodic feature is observed on the return scan of $Co^{II}(dmgBF_2)_2(CH_3CN)_2$, suggesting a CoH resting state. A critical aspect here is that the formal oxidation state of the catalytic intermediate cannot be definitively assigned without knowing the fate of the $Co^{III}H$

DOI: 10.1021/jacs.6b04779
J. Am. Chem. Soc. 2016, 138, 8309−8318

intermediate on the forward scan. For example, Lomoth, Ott and co-workers observed a similar anodic feature in studies on a polypyridyl cobalt electrocatalyst, and assigned the wave to oxidation of a $Co^{III}H$ intermediate.[22] A different conclusion was reached in a recent study from Dempsey and co-workers, who attributed the anodic feature of $Co^{II}(dmgBF_2)_2(CH_3CN)_2$ to oxidation of a $Co^{II}H$ intermediate.[71,72] Here we have used FOWA to show that the $Co^{III}H$ intermediate of $Co^{II}(dmgBF_2)_2(CH_3CN)_2$ is reduced on the forward scan through the catalytic wave, providing clear evidence supporting Dempsey's conclusion that the anodic feature corresponds to oxidation of a $Co^{II}H$ resting state.

Notably, our use of FOWA differs from its originally prescribed purpose of measuring kinetic data at the onset of the catalytic wave where competing side phenomena are absent.[56] In our FOWA approach, the presence of non-ideal behavior at the catalytic onset is used to identify the reaction sequence for catalysts having closely spaced redox couples. We have recently employed FOWA in this manner to observe a key intermediate in the production of H_2 by $[Ni(P^{Ph}_2N^{Ph}_2)_2]^{2+}$,[62] and this FOWA strategy was a key factor in identification of $Co^{III}H$ reduction waves in the present study. These findings indicate that FOWA has additional valuable applications beyond the direct measurement of chemical rate constants.

The observation of quasireversible electron-transfer kinetics for the second reduction step in the catalytic pathway provides further support for assignment of the transient intermediates as $Co^{III}H$. Significant reorganization of the inner coordination sphere is expected for reduction of low-spin Co^{III} (d^6) to low-spin Co^{II} (d^7) by outer-sphere electron transfer. Consistent with this expectation, a slow $Co^{III/II}$ electron-transfer self-exchange rate was measured for a cobaloxime derivative,[73] and quasireversible electrode kinetics have been measured for some isolated $Co^{III}H$ complexes.[39,57] Electron transfer is not necessarily a discrete reaction step, and the kinetics of solvent binding and dissociation for both Co^{III} and Co^{II} are likely to have a major impact on the observed electrode kinetics (see SI for further discussion).[57]

Catalyst Comparison. In the present study, the pK_a of the acid used for electrocatalysis is closely matched to the pK_a of $Co^{III}H$ for both catalysts. As a result, protonation of Co^{I} is essentially thermoneutral, while protonation of $Co^{II}H$ to make H_2 is exergonic. Considering their similar thermodynamic properties, comparison of the overpotentials for $[Co^{II}(P^{tBu}_2N^{Ph}_2)(CH_3CN)_3]^{2+}$ and $Co^{II}(dmgBF_2)_2(CH_3CN)_2$ is informative. Here we use the traditional practice of reporting the overpotential at the catalytic half-wave potential ($\eta_{cat/2}$)[74] using the potential of the H^+/H_2 couple in acetonitrile ($E^\circ_{H+} = -0.028$ V)[75] and the pK_a of the acid used for catalysis (eq 7).

$$\eta_{cat/2} = E^\circ_{H^+} - 0.059 \times \log(pK_a) - E_{cat/2} \quad (7)$$

In this manner, $\eta_{cat/2}$ is calculated to be 300 mV for $[Co^{II}(P^{tBu}_2N^{Ph}_2)(CH_3CN)_3]^{2+}$ using *p*-bromoanilinium (pK_a = 9.4)[61] and 180 mV for $Co^{II}(dmgBF_2)_2(CH_3CN)_2$ using anilinium (pK_a = 10.6).[61] These overpotentials are larger than previously reported[7,9,44] due to our use of the more recent $E^\circ_{H^+}$ value determined from accurate open-circuit potential measurements.[75] For an ECEC mechanism, the difference between $E_{cat/2}$ and $E^{\circ\prime}$ of the non-catalytic wave results from the difference in the rate constants for the two chemical steps of catalysis (eq 8).[54] The difference in overpotential between the two

$$E_{cat/2} = E^{\circ\prime} + \frac{RT}{F}\ln\left(1 + \frac{\sqrt{k_1}}{\sqrt{k_2}}\right) \quad (8)$$

catalysts stems mostly from a difference in the rate-determining steps. Protonation of Co^{I} (k_1) is rate-limiting in catalysis by $[Co^{II}(P^{tBu}_2N^{Ph}_2)(CH_3CN)_3]^{2+}$, so $E_{cat/2}$ is equal to $E^{\circ\prime}$. In contrast, protonation of $Co^{II}H$ to make H_2 (k_2) is rate-limiting for $Co^{II}(dmgBF_2)_2(CH_3CN)_2$, so $E_{cat/2}$ is shifted positive of $E^{\circ\prime}$ and the $\eta_{cat/2}$ is decreased.

A key factor contributing to the modest $\eta_{cat/2}$ values of these catalysts is the proximity of their $Co^{II/I}$ and $Co^{III/II}H$ couples, which allows both electron transfers required for catalysis to occur at similar potentials. Understanding how to control $\Delta E^{\circ\prime}$ will help facilitate the design of efficient electrocatalysts. Thermodynamic data for $[HCo^{III}(P^{tBu}_2N^{Ph}_2)(CH_3CN)_3]^{2+}$, $HCo^{III}(dmgBF_2)_2(CH_3CN)$, and other $Co^{III}H$ complexes having known bond strengths is tabulated in Table 1. The entries in Table 1 are arranged in order of decreasing $\Delta E^{\circ\prime}$, where a postive value of $\Delta E^{\circ\prime}$ indicates that the $Co^{III/II}H$ couple is more positive than the $Co^{II/I}$ couple. Moderate correlations are observed between $\Delta E^{\circ\prime}$ and the hydride donor ability of $Co^{II}H$, the BDFE of $Co^{III}H$, and the BDFE of $Co^{II}H$ (SI, Figures S18–S20). A stronger correlation is observed between $\Delta E^{\circ\prime}$ and the pK_a of $Co^{III}H$ (Figure 7), suggesting that the use of weaker electron donor ligands causes a greater shift in the $Co^{III/II}H$ couple than in the $Co^{II/I}$ couple. Geometric factors can also play a role, as $[HCo^{III}(5P_4N_2)(CH_3CN)]^{2+}$ is 2.5 pK_a units less acidic than $[HCo^{III}(6P_4N_2)(CH_3CN)]^{2+}$, even though the complexes differ only in the chelate size of their tetradentate phosphine ligands.[40]

These findings suggest that $\Delta E^{\circ\prime}$ can be tuned by controlling the pK_a of the $Co^{III}H$ intermediate. A pK_a of 8.0 has been reported for $[HCo^{III}(triphos)(CH_3CN)_2]^{2+}$ (triphos = $CH_3C(C_2H_4PPh_2)_3$),[42] leading to a prediction that the $Co^{III/II}H$ couple is 450 mV more positive than the $Co^{II/I}$ couple. This estimate does not match well with the experimentally observed $Co^{III}H$ reduction wave, which appears ~180 mV more negative than the $Co^{II/I}$ couple. It must be noted that the *observed* $Co^{III}H$

Table 1. Thermochemical Data for $Co^{III}H$ and $Co^{II}H$ Complexes

complex	$E^{\circ\prime}(Co^{III/II}H) - E^{\circ\prime}(Co^{II/I})$ (V)	$pK_a(Co^{III}H)$	$\Delta G^\circ_{H^-}(Co^{II}H)$ (kcal mol^{-1})	$\Delta G^\circ_{H^\bullet}(Co^{III}H)$ (kcal mol^{-1})	$\Delta G^\circ_{H^\bullet}(Co^{II}H)$ (kcal mol^{-1})	ref
$HCo^{III}(dmgBF_2)_2(CH_3CN)$	0.16	10.7	55.9	47.2	50.9	this work
$[HCo^{III}(P^{tBu}_2N^{Ph}_2)(CH_3CN)_3]^{2+}$	0.07	9.7	54.2	46.8	48.4	this work
$[HCo^{III}(dppe)_2(CH_3CN)]^{2+}$	−0.13	11.9	59.7	53.7	50.7	40, 68
$[HCo^{III}(6P_4N_2)(CH_3CN)]^{2+}$ [a]	−0.45	13.5	50.5	53.1	43.4	40
$[HCo^{III}(Cp^{C_5H_4N})(P^{tBu}_2N^{Ph}_2)]^{+}$ [b]	−0.66	15.6	41.9	53.0	37.8	39
$[HCo^{III}(5P_4N_2)(CH_3CN)]^{2+}$ [c]	−0.73	16.0	46.8	56.5	39.7	40

[a] $6P_4N_2$ = 1,5-diphenyl-3,7-bis(diphenylphosphino)propyl-1,5-diaza-3,7-diphosphacyclooctane. [b] $Cp^{C_5H_4N}$ = (tetrafluoropyridyl)cyclopentadienide. [c] $5P_4N_2$ = 1,5-diphenyl-3,7-bis(diphenylphosphino)ethyl-1,5-diaza-3,7-diphosphacyclooctane.

DOI: 10.1021/jacs.6b04779
J. Am. Chem. Soc. 2016, 138, 8309–8318

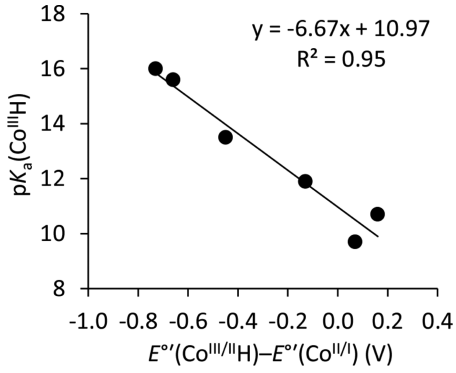

Figure 7. Plot of pK_a ($Co^{III}H$) versus $E^{\circ\prime}(Co^{III/II}H) - E^{\circ\prime}(Co^{II/I})$ for the complexes tabulated in Table 1.

reduction potential is not necessarily equal to the *formal* $Co^{III/II}H$ couple ($E^{\circ\prime}$). This point is illustrated by $[HCo^{III}(dppe)_2(CH_3CN)]^{2+}$, which displays a cathodic peak potential that is 190 mV more negative than that of the formal $Co^{III/II}H$ couple.[68]

CONCLUSIONS

We have demonstrated that transient cobalt hydride intermediates of electrocatalytic H_2 prodcution by $[Co^{II}(P^{tBu}{}_2N^{Ph}{}_2)(CH_3CN)_3](BF_4)_2$ and $Co^{II}(dmgBF_2)_2(CH_3CN)_2$ can be identified using variable scan rate cyclic voltammetry and foot-of-the-wave analysis. These simple, yet powerful, techniques were critical for identifying the reduction of transient $Co^{III}H$ intermediates under electrocatalytic conditions. The observation of quasi-reversible electron-transfer kinetics supported the identification of the transient intermediates as $Co^{III}H$. In the case of $Co^{II}(dmgBF_2)_2(CH_3CN)_2$, a bridge-protonated Co^{I} complex was ruled out as a catalytic intermediate by recording CVs of Co^{II} at 1000 psi of H_2. Computational analysis revealed that both catalysts have very similar Co−H bond strengths, despite having very different ligand sets. Importantly, both compounds display a low overpotential for catalytic H_2 production, due largely to the proximity of the $Co^{II/I}$ and $Co^{III/II}H$ couples.[42] Comparison to other electrocatalysts reveals that the separation between the $Co^{II/I}$ and $Co^{III/II}H$ couples can be controlled by tuning the pK_a of the $Co^{III}H$; this design approach could prove fruitful in future design of improved electrocatalysts

The electrochemical methods presented in this work provide an easily accessible, widely applicable tool for analysis of mechanisms. In conjuction with recent electrochemical methods from Costentin and Savéant, information on catalytic mechanisms can be gained directly from the catalytic voltammograms without relying soley on computation or specialized spectroscopic techniques. Thus, the approaches outlined in this work are poised to become valuable tools in the analyis of a wide variety of molecular electrocatalysts.

EXPERIMENTAL SECTION

Methods and Materials. All manipulations were carried out under N_2 using standard Schlenk and inert atmosphere glovebox techniques. Acetonitrile (Alfa-Aesar, anhydrous, amine-free) was purified by sparging with N_2 and passage through neutral alumina using an Innovative Technology, Inc., Pure Solv solvent purification system. Tetrabutylammonium tetrafluoroborate was recrystallized from CH_3CN and dried under vacuum. Anilinium salts were prepared by reaction of the substituted aniline with 1.5 equiv of $HBF_4{\cdot}Et_2O$ followed by recrystallization from CH_3CN/Et_2O. Water was dispensed from a Millipore Milli-Q purifier and sparged with nitrogen. Ferrocene was sublimed under vacuum. Hydrogen (UHP grade) was dried and deoxygenated by passage through in-line scrubbers (Agilent OT-4-SS). The complexes $[Co^{II}(P^{tBu}{}_2N^{Ph}{}_2)(CH_3CN)_3](BF_4)_2$[44] and $Co^{II}(dmgBF_2)_2(H_2O)_2$[76] were prepared according to literature procedures. $Co^{II}(dmgBF_2)_2(CH_3CN)_2$ is formed upon dissolution of $Co^{II}(dmgBF_2)_2(H_2O)_2$ in acetonitrile.[77]

Electrochemistry. Voltammetry measurements were performed using a CH Instruments 600D or 620D potentiostat equipped with a standard three-electrode cell. Experiments were performed in a glovebox at ambient temperature, 23 ± 2 °C, using a 3−5 mL conical glass vial fitted with a polysilicone cap having openings sized to closely accept each electrode. The working electrode (1 mm PEEK-encased glassy carbon disc, ALS) was polished using diamond paste (Buehler, 0.25 μm) on a polishing pad wet with purified H_2O, then the electrode was rinsed with neat acetonitrile. A glassy carbon rod (Structure Probe, Inc.) was used as the counterelectrode, and a silver wire suspended in a solution of Bu_4NBF_4 (0.2 M) in acetonitrile and separated from the analyte solution by a Vycor frit (CH Instruments 112) was used a pseudoreference electrode. Ferrocene was added as an internal standard, and all potentials are referenced to the $Cp_2Fe^{+/0}$ couple at 0 V.

The uncompensated solution resistance (R_u) under these conditions was determined to be <50 Ω using the built-in *iR* compensation feature of the potentiostat. *iR* compensation was not enabled in the collection of electrochemical data since R_u is small relative to the maximum peak currents measured (<20 μA). The potential error resulting from uncompensated resistance is ≤1 mV.

For FOWA, voltammograms were background-subtracted by extrapolation of the non-Faradaic charging current observed at the beginning of the potential scan. The $E_{cat/2}$ values used in FOWA were identified from the first-derivative trace by finding the potential of the first maximum. The $E_{cat/2}$ values fell in the linear region of the resulting FOWA plots, indicating that substrate depletion did not affect the measurement of $E_{cat/2}$.

High-Pressure Electrochemistry. ***Caution*** *should be used when performing reactions under pressure!* The system should be designed such that each component is rated to a higher pressure than the experimentally desired pressure, and a pressure-relief fail-safe should be incorporated in case of an accidental overpressurization. Voltammetry was performed at elevated H_2 pressure using a commercially available pressure reactor (Parr Instrument Co. 4793Q) equipped with two 4-lead signal feedthroughs (Conax Technologies MTG-24T(CU)-A4-T). A glass cell was placed within the reactor and loaded with the reaction solution and a cross-shaped stirbar. A custom fabricated cell cap vented to the interior of the reactor was used to position six pre-polished glassy carbon working electrodes, a glassy carbon rod counterelectrode, and a bare platinum wire reference electrode within the analyte solution. A schematic of this cell configuration has been previously reported.[78]

In a typical experiment, the reactor was charged with 10 mL of acetontrile solution (0.2 M NBu_4PF_6) containing $Co^{II}(dmgBF_2)_2(CH_3CN)_2$ (1 mM) and ferrocene (0.5 mM). The assembled reactor was attached to the pressure assembly, and the gas line was flushed with H_2. The reactor was pressurized to 1000 psi H_2 while stirring, then vented to displace the N_2. This process was repeated three times, then the reactor was sealed under H_2 pressure and voltammograms were recorded at periodic intervals. After releasing the gas pressure, the reactor was taken into a glovebox and disassembled to facilitate the loss of H_2 from the solution. Voltammograms were recorded periodically to monitor the conversion of the product back into starting material.

Computational Details. All calculations were carried out with the program Gaussian 09.[79] Each structure was optimized without symmetry constraint using the B3P86 functional.[80,81] The Stuttgart basis set with effective core potential (ECP)[82] was used for the Co atom, and the 6-31G* basis set[83,84] was used for the remaining atoms with one additional *p* polarization function [$\xi(p) = 1.1$] for hydride ligands. A frequency calculation was performed on each structure at the same level of theory in order to confirm that the structure was a real local minimum on the potential energy surface. Free energy was calculated in the gas phase at 298 K in the harmonic approximation.

DOI: 10.1021/jacs.6b04779
J. Am. Chem. Soc. 2016, 138, 8309−8318

Acetonitrile solvation free energies were calculated with the polarizable continuum model (C-PCM)[85,86] using Bondi[87] atomic radii. Several different structural isomers were calculated for derivatives of $[Co^{II}(P^{tBu}{}_2N^{Ph}{}_2)(CH_3CN)_3]^{2+}$, and the free energy of the most stable isomers were used in the isodesmic calculations. Computational data for the $[Co(dppe)_2]^{n+}$ reference system at an identical level of theory have been previously reported.[40]

■ ASSOCIATED CONTENT

Supporting Information

The Supporting Information is available free of charge on the ACS Publications website at DOI: 10.1021/jacs.6b04779.

Details on measurement of electron-transfer kinetic parameters, additional voltammograms, energies from DFT calculations, thermochemical cycles, correlation of reduction potentials and heterolytic/homolytic Co−H bond strengths, and XYZ coordinates for geometry optimized structures (PDF)

■ AUTHOR INFORMATION

Corresponding Author

*eric.wiedner@pnnl.gov

Notes

The authors declare no competing financial interest.

■ ACKNOWLEDGMENTS

We thank Dr. Monte Helm and Dr. Aaron Appel for helpful discussions. This research was supported as part of the Center for Molecular Electrocatalysis, an Energy Frontier Research Center funded by the U.S. Department of Energy, Office of Science, Office of Basic Energy Sciences. Computational resources were provided at the National Energy Research Scientific Computing Center (NERSC) at Lawrence Berkeley National Laboratory. Pacific Northwest National Laboratory is operated by Battelle for the U.S. Department of Energy.

■ REFERENCES

(1) Artero, V.; Chavarot-Kerlidou, M.; Fontecave, M. *Angew. Chem., Int. Ed.* **2011**, *50*, 7238−7266.
(2) Du, P.; Eisenberg, R. *Energy Environ. Sci.* **2012**, *5*, 6012−6021.
(3) Eckenhoff, W. T.; McNamara, W. R.; Du, P.; Eisenberg, R. *Biochim. Biophys. Acta, Bioenerg.* **2013**, *1827*, 958−973.
(4) Dempsey, J. L.; Brunschwig, B. S.; Winkler, J. R.; Gray, H. B. *Acc. Chem. Res.* **2009**, *42*, 1995−2004.
(5) Thoi, V. S.; Sun, Y.; Long, J. R.; Chang, C. J. *Chem. Soc. Rev.* **2013**, *42*, 2388−2400.
(6) McKone, J. R.; Marinescu, S. C.; Brunschwig, B. S.; Winkler, J. R.; Gray, H. B. *Chem. Sci.* **2014**, *5*, 865−878.
(7) Hu, X. L.; Brunschwig, B. S.; Peters, J. C. *J. Am. Chem. Soc.* **2007**, *129*, 8988−8998.
(8) Jacques, P. A.; Artero, V.; Pecaut, J.; Fontecave, M. *Proc. Natl. Acad. Sci. U. S. A.* **2009**, *106*, 20627−20632.
(9) Baffert, C.; Artero, V.; Fontecave, M. *Inorg. Chem.* **2007**, *46*, 1817−1824.
(10) Chen, L.; Wang, M.; Han, K.; Zhang, P.; Gloaguen, F.; Sun, L. *Energy Environ. Sci.* **2014**, *7*, 329−334.
(11) van der Meer, M.; Glais, E.; Siewert, I.; Sarkar, B. *Angew. Chem., Int. Ed.* **2015**, *54*, 13792−13795.
(12) McCrory, C. C. L.; Uyeda, C.; Peters, J. C. *J. Am. Chem. Soc.* **2012**, *134*, 3164−3170.
(13) Stubbert, B. D.; Peters, J. C.; Gray, H. B. *J. Am. Chem. Soc.* **2011**, *133*, 18070−18073.
(14) Khnayzer, R. S.; Thoi, V. S.; Nippe, M.; King, A. E.; Jurss, J. W.; El Roz, K. A.; Long, J. R.; Chang, C. J.; Castellano, F. N. *Energy Environ. Sci.* **2014**, *7*, 1477−1488.
(15) Bigi, J. P.; Hanna, T. E.; Harman, W. H.; Chang, A.; Chang, C. J. *Chem. Commun.* **2010**, *46*, 958−960.
(16) Shan, B.; Baine, T.; Ma, X. A. N.; Zhao, X.; Schmehl, R. H. *Inorg. Chem.* **2013**, *52*, 4853−4859.
(17) Singh, W. M.; Baine, T.; Kudo, S.; Tian, S.; Ma, X. A. N.; Zhou, H.; DeYonker, N. J.; Pham, T. C.; Bollinger, J. C.; Baker, D. L.; Yan, B.; Webster, C. E.; Zhao, X. *Angew. Chem., Int. Ed.* **2012**, *51*, 5941−5944.
(18) McNamara, W. R.; Han, Z. J.; Yin, C. J.; Brennessel, W. W.; Holland, P. L.; Eisenberg, R. *Proc. Natl. Acad. Sci. U. S. A.* **2012**, *109*, 15594−15599.
(19) Lazarides, T.; McCormick, T.; Du, P.; Luo, G.; Lindley, B.; Eisenberg, R. *J. Am. Chem. Soc.* **2009**, *131*, 9192−9194.
(20) Szajna-Fuller, E.; Bakac, A. *Eur. J. Inorg. Chem.* **2010**, *2010*, 2488−2494.
(21) Tong, L.; Zong, R.; Thummel, R. P. *J. Am. Chem. Soc.* **2014**, *136*, 4881−4884.
(22) Singh, W. M.; Mirmohades, M.; Jane, R. T.; White, T. A.; Hammarstrom, L.; Thapper, A.; Lomoth, R.; Ott, S. *Chem. Commun.* **2013**, *49*, 8638−8640.
(23) Wakerley, D. W.; Reisner, E. *Phys. Chem. Chem. Phys.* **2014**, *16*, 5739−5746.
(24) Wakerley, D. W.; Reisner, E. *Energy Environ. Sci.* **2015**, *8*, 2283−2295.
(25) Mondal, B.; Sengupta, K.; Rana, A.; Mahammed, A.; Botoshansky, M.; Dey, S. G.; Gross, Z.; Dey, A. *Inorg. Chem.* **2013**, *52*, 3381−3387.
(26) Kleingardner, J. G.; Kandemir, B.; Bren, K. L. *J. Am. Chem. Soc.* **2014**, *136*, 4−7.
(27) Muresan, N. M.; Willkomm, J.; Mersch, D.; Vaynzof, Y.; Reisner, E. *Angew. Chem., Int. Ed.* **2012**, *51*, 12749−12753.
(28) Andreiadis, E. S.; Jacques, P.-A.; Tran, P. D.; Leyris, A.; Chavarot-Kerlidou, M.; Jousselme, B.; Matheron, M.; Pécaut, J.; Palacin, S.; Fontecave, M.; Artero, V. *Nat. Chem.* **2013**, *5*, 48−53.
(29) Krawicz, A.; Yang, J.; Anzenberg, E.; Yano, J.; Sharp, I. D.; Moore, G. F. *J. Am. Chem. Soc.* **2013**, *135*, 11861−11868.
(30) Krawicz, A.; Cedeno, D.; Moore, G. F. *Phys. Chem. Chem. Phys.* **2014**, *16*, 15818−15824.
(31) Kaeffer, N.; Chavarot-Kerlidou, M.; Artero, V. *Acc. Chem. Res.* **2015**, *48*, 1286−1295.
(32) Fihri, A.; Artero, V.; Razavet, M.; Baffert, C.; Leibl, W.; Fontecave, M. *Angew. Chem., Int. Ed.* **2008**, *47*, 564−567.
(33) Zhang, P.; Wang, M.; Li, C.; Li, X.; Dong, J.; Sun, L. *Chem. Commun.* **2009**, *46*, 8806−8808.
(34) Jasimuddin, S.; Yamada, T.; Fukuju, K.; Otsuki, J.; Sakai, K. *Chem. Commun.* **2010**, *46*, 8466−8468.
(35) Veldkamp, B. S.; Han, W.-S.; Dyar, S. M.; Eaton, S. W.; Ratner, M. A.; Wasielewski, M. R. *Energy Environ. Sci.* **2013**, *6*, 1917−1928.
(36) Huang, J.; Mulfort, K. L.; Du, P.; Chen, L. X. *J. Am. Chem. Soc.* **2012**, *134*, 16472−16475.
(37) Utschig, L. M.; Silver, S. C.; Mulfort, K. L.; Tiede, D. M. *J. Am. Chem. Soc.* **2011**, *133*, 16334−16337.
(38) Koelle, U.; Paul, S. *Inorg. Chem.* **1986**, *25*, 2689−2694.
(39) Fang, M.; Wiedner, E. S.; Dougherty, W. G.; Kassel, W. S.; Liu, T.; DuBois, D. L.; Bullock, R. M. *Organometallics* **2014**, *33*, 5820−5833.
(40) Wiedner, E. S.; Appel, A. M.; DuBois, D. L.; Bullock, R. M. *Inorg. Chem.* **2013**, *52*, 14391−14403.
(41) Lee, C. H.; Dogutan, D. K.; Nocera, D. G. *J. Am. Chem. Soc.* **2011**, *133*, 8775−8777.
(42) Marinescu, S. C.; Winkler, J. R.; Gray, H. B. *Proc. Natl. Acad. Sci. U. S. A.* **2012**, *109*, 15127−15131.
(43) Jacobsen, G. M.; Yang, J. Y.; Twamley, B.; Wilson, A. D.; Bullock, R. M.; Rakowski DuBois, M.; DuBois, D. L. *Energy Environ. Sci.* **2008**, *1*, 167−174.
(44) Wiedner, E. S.; Yang, J. Y.; Dougherty, W. G.; Kassel, W. S.; Bullock, R. M.; Rakowski DuBois, M.; DuBois, D. L. *Organometallics* **2010**, *29*, 5390−5401.

DOI: 10.1021/jacs.6b04779
J. Am. Chem. Soc. 2016, 138, 8309−8318

(45) Hu, X. L.; Cossairt, B. M.; Brunschwig, B. S.; Lewis, N. S.; Peters, J. C. *Chem. Commun.* **2005**, 4723−4725.
(46) Razavet, M.; Artero, V.; Fontecave, M. *Inorg. Chem.* **2005**, *44*, 4786−4795.
(47) King, A. E.; Surendranath, Y.; Piro, N. A.; Bigi, J. P.; Long, J. R.; Chang, C. J. *Chem. Sci.* **2013**, *4*, 1578−1587.
(48) Sun, Y.; Bigi, J. P.; Piro, N. A.; Tang, M. L.; Long, J. R.; Chang, C. J. *J. Am. Chem. Soc.* **2011**, *133*, 9212−9215.
(49) Muckerman, J. T.; Fujita, E. *Chem. Commun.* **2011**, *47*, 12456−12458.
(50) Solis, B. H.; Hammes-Schiffer, S. *Inorg. Chem.* **2011**, *50*, 11252−11262.
(51) Dempsey, J. L.; Winkler, J. R.; Gray, H. B. *J. Am. Chem. Soc.* **2010**, *132*, 16774−16776.
(52) Estes, D. P.; Grills, D. C.; Norton, J. R. *J. Am. Chem. Soc.* **2014**, *136*, 17362−17365.
(53) Lacy, D. C.; Roberts, G. M.; Peters, J. C. *J. Am. Chem. Soc.* **2015**, *137*, 4860−4864.
(54) Costentin, C.; Savéant, J. M. *ChemElectroChem* **2014**, *1*, 1226−1236.
(55) Costentin, C.; Dridi, H.; Savéant, J. M. *J. Am. Chem. Soc.* **2014**, *136*, 13727−13734.
(56) Costentin, C.; Drouet, S.; Robert, M.; Savéant, J. M. *J. Am. Chem. Soc.* **2012**, *134*, 11235−11242.
(57) Wiedner, E. S.; Roberts, J. A. S.; Dougherty, W. G.; Kassel, W. S.; DuBois, D. L.; Bullock, R. M. *Inorg. Chem.* **2013**, *52*, 9975−9988.
(58) Bard, A. J.; Faulkner, L. R. *Electrochemical Methods: Fundamentals and Applications*, 2nd ed.; John Wiley & Sons: Hoboken, NJ, 2001.
(59) Savéant, J. M. *Elements of Molecular and Biomolecular Electrochemistry: An Electrochemical Approach to Election Transfer Chemistry*; Wiley: New York, 2006.
(60) Mashkina, E.; Bond, A. M. *Anal. Chem.* **2011**, *83*, 1791−1799.
(61) Kaljurand, I.; Kutt, A.; Soovali, L.; Rodima, T.; Maemets, V.; Leito, I.; Koppel, I. A. *J. Org. Chem.* **2005**, *70*, 1019−1028.
(62) Wiedner, E. S.; Brown, H. J. S.; Helm, M. L. *J. Am. Chem. Soc.* **2016**, *138*, 604−616.
(63) Costa, G.; Tavagnacco, C.; Puxeddu, A.; Balducci, G.; Kumar, R. *J. Organomet. Chem.* **1987**, *330*, 185−199.
(64) Parker, V. D.; Handoo, K. L.; Roness, F.; Tilset, M. *J. Am. Chem. Soc.* **1991**, *113*, 7493−7498.
(65) Qi, X.-J.; Fu, Y.; Liu, L.; Guo, Q.-X. *Organometallics* **2007**, *26*, 4197−4203.
(66) Qi, X.-J.; Liu, L.; Fu, Y.; Guo, Q.-X. *Organometallics* **2006**, *25*, 5879−5886.
(67) Chen, S.; Rousseau, R.; Raugei, S.; Dupuis, M.; DuBois, D. L.; Bullock, R. M. *Organometallics* **2011**, *30*, 6108−6118.
(68) Ciancanelli, R.; Noll, B. C.; DuBois, D. L.; Rakowski DuBois, M. *J. Am. Chem. Soc.* **2002**, *124*, 2984−2992.
(69) Wayner, D. D. M.; Parker, V. D. *Acc. Chem. Res.* **1993**, *26*, 287−294.
(70) Ellis, W. W.; Raebiger, J. W.; Curtis, C. J.; Bruno, J. W.; DuBois, D. L. *J. Am. Chem. Soc.* **2004**, *126*, 2738−2743.
(71) Rountree, E. S.; Martin, D. J.; McCarthy, B. D.; Dempsey, J. L. *ACS Catal.* **2016**, *6*, 3326−3335.
(72) Martin, D. J.; McCarthy, B. D.; Rountree, E. S.; Dempsey, J. L. *Dalton Trans.* **2016**, *45*, 9970−9976.
(73) Dempsey, J. L.; Winkler, J. R.; Gray, H. B. *J. Am. Chem. Soc.* **2010**, *132*, 1060−1065.
(74) Felton, G. A. N.; Glass, R. S.; Lichtenberger, D. L.; Evans, D. H. *Inorg. Chem.* **2006**, *45*, 9181−9184.
(75) Roberts, J. A. S.; Bullock, R. M. *Inorg. Chem.* **2013**, *52*, 3823−3835.
(76) Bakac, A.; Espenson, J. H. *J. Am. Chem. Soc.* **1984**, *106*, 5197−5202.
(77) Li, G.; Estes, D. P.; Norton, J. R.; Ruccolo, S.; Sattler, A.; Sattler, W. *Inorg. Chem.* **2014**, *53*, 10743−10747.
(78) Dutta, A.; Roberts, J. A. S.; Shaw, W. J. *Angew. Chem., Int. Ed.* **2014**, *53*, 6487−6491.
(79) Frisch, M. J.; Trucks, G. W.; Schlegel, H. B.; Scuseria, G. E.; Robb, M. A.; Cheeseman, J. R.; Scalmani, G.; Barone, V.; Mennucci, B.; Petersson, G. A.; Nakatsuji, H.; Caricato, M.; Li, X.; Hratchian, H. P.; Izmaylov, A. F.; Bloino, J.; Zheng, G.; Sonnenberg, J. L.; Hada, M.; Ehara, M.; Toyota, K.; Fukuda, R.; Hasegawa, J.; Ishida, M.; Nakajima, T.; Honda, Y.; Kitao, O.; Nakai, H.; Vreven, T.; Montgomery, J. A., Jr.; Peralta, J. E.; Ogliaro, F.; Bearpark, M.; Heyd, J. J.; Brothers, E.; Kudin, K. N.; Staroverov, V. N.; Kobayashi, R.; Normand, J.; Raghavachari, K.; Rendell, A.; Burant, J. C.; Iyengar, S. S.; Tomasi, J.; Cossi, M.; Rega, N.; Millam, J. M.; Klene, M.; Knox, J. E.; Cross, J. B.; Bakken, V.; Adamo, C.; Jaramillo, J.; Gomperts, R.; Stratmann, R. E.; Yazyev, O.; Austin, A. J.; Cammi, R.; Pomelli, C.; Ochterski, J. W.; Martin, R. L.; Morokuma, K.; Zakrzewski, V. G.; Voth, G. A.; Salvador, P.; Dannenberg, J. J.; Dapprich, S. A.; Daniels, D.; Farkas, O.; Foresman, J. B.; Ortiz, J. V.; Cioslowski, J.; Fox, D. J. *Gaussian 09*, Revision B.01; Gaussian, Inc.: Wallingford, CT, 2010.
(80) Becke, A. D. *J. Chem. Phys.* **1993**, *98*, 5648−5652.
(81) Perdew, J. P. *Phys. Rev. B: Condens. Matter Mater. Phys.* **1986**, *33*, 8822−8824.
(82) Andrae, D.; Haussermann, U.; Dolg, M.; Stoll, H.; Preuss, H. *Theor. Chem. Acc.* **1990**, *77*, 123−141.
(83) Francl, M. M.; Pietro, W. J.; Hehre, W. J.; Binkley, J. S.; Gordon, M. S.; Defrees, D. J.; Pople, J. A. *J. Chem. Phys.* **1982**, *77*, 3654−3665.
(84) Rassolov, V. A.; Ratner, M. A.; Pople, J. A.; Redfern, P. C.; Curtiss, L. A. *J. Comput. Chem.* **2001**, *22*, 976−984.
(85) Barone, V.; Cossi, M. *J. Phys. Chem. A* **1998**, *102*, 1995−2001.
(86) Cossi, M.; Rega, N.; Scalmani, G.; Barone, V. *J. Comput. Chem.* **2003**, *24*, 669−681.
(87) Bondi, A. *J. Phys. Chem.* **1964**, *68*, 441−451.

DOI: 10.1021/jacs.6b04779
J. Am. Chem. Soc. 2016, 138, 8309−8318